OXFORD

Cerebral Cortex, 2024, **34**, 1–12
https://doi.org/10.1093/cercor/bhad394
Advance access publication date 9 November 2023
Original Article

Direct interhemispheric cortical communication via thalamic commissures: a new white matter pathway in the primate brain

Diego Szczupak[1], David J. Schaeffer[1], Xiaoguang Tian[1], Sang-Ho Choi[1], Fang-Cheng[2], Pamela Meneses Iack[3], Vinicius P. Campos[4], J. Patrick Mayo[5], Janina Patsch[6], Christian Mitter[6], Amit Haboosheh[7], Ha Seung Kwon[1], Marcelo A.C. Vieira[4], Daniel S. Reich[8], Steve Jacobson[8], Gregor Kasprian[6], Fernanda Tovar-Moll[9], Roberto Lent[3,9], Afonso C. Silva[1,*]

[1]University of Pittsburgh Brain Institute, Department of Neurobiology, University of Pittsburgh, 3501 Fifth Avenue, Pittsburgh, PA 15261, USA,
[2]Department of Neurological Surgery, University of Pittsburgh, 200 Lothrop Street, Pittsburgh, PA 15261, USA,
[3]Biomedical Sciences Institute, Federal University of Rio de Janeiro, 373 Carlos Chagas Filho Avenue, Rio de Janeiro, Rio de Janeiro 21941-853, Brazil,
[4]Department of Electrical and Computer Engineering, 400 Trabalhador São-Carlense Avenue, University of São Paulo, São Carlos, SP 13565-905, Brazil,
[5]Department of Ophthalmology, University of Pittsburgh, 1622 Locust Street, Pittsburgh, PA 15261, USA,
[6]Department of Biomedical Imaging and Image-Guided Therapy of the Medical University of Vienna, 18-20 Währinger Gürtel, 1090, Vienna, Austria,
[7]Department of Radiology Hadassah Ein Karem Hospital, Kalman Ya'akov Man St, Jerusalem 9112001, Israel,
[8]National Institute of Neurological Disorders and Stroke, National Institutes of Health, 10 Center Drive, Bethesda, MD 20814, USA,
[9]D'Or Institute of Research and Education, 30 Rua Diniz Cordeiro Street, Rio de Janeiro, Rio de Janeiro 22281-100, Brazil

*Corresponding author: Department of Neurobiology, University of Pittsburgh Brain Institute. 3501 Fifth Avenue #3058, 3058 Biomedical Science Tower 3, Pittsburgh, PA 15261, United States. Email: afonso@pitt.edu

Cortical neurons of eutherian mammals project to the contralateral hemisphere, crossing the midline primarily via the corpus callosum and the anterior, posterior, and hippocampal commissures. We recently reported and named the thalamic commissures (TCs) as an additional interhemispheric axonal fiber pathway connecting the cortex to the contralateral thalamus in the rodent brain. Here, we demonstrate that TCs also exist in primates and characterize the connectivity of these pathways with high-resolution diffusion-weighted MRI, viral axonal tracing, and fMRI. We present evidence of TCs in both New World (*Callithrix jacchus* and *Cebus apella*) and Old World primates (*Macaca mulatta*). Further, like rodents, we show that the TCs in primates develop during the embryonic period, forming anatomical and functionally active connections of the cortex with the contralateral thalamus. We also searched for TCs in the human brain, showing their presence in humans with brain malformations, although we could not identify TCs in healthy subjects. These results pose the TCs as a vital fiber pathway in the primate brain, allowing for more robust interhemispheric connectivity and synchrony and serving as an alternative commissural route in developmental brain malformations.

Key words: marmoset; primate; thalamic commissures; corpus callosum; diffusion imaging.

Introduction

The eutherian mammalian brain has evolved to cluster neurons in specific brain regions that perform distinct functions, interconnected so that the whole is greater than the sum of its individual parts (Schaeffer et al. 2020). These connections can be categorized as intrahemispheric, occurring within a cerebral hemisphere, or interhemispheric, crossing the midline through specific pathways. The corpus callosum (CC) is the main interhemispheric pathway in the Eutherian mammalian brain, followed by the anterior, posterior, and hippocampal commissures (Suárez et al. 2014; Suárez et al. 2018).

Recently, we discovered a novel interhemispheric axonal fiber pathway in rodents connecting the cortex with the contralateral thalamus, which we named as the thalamic commissures (TCs), formed by 4 distinct patches traversing the thalamus midline (Szczupak, Iack, et al. 2021). These findings support previous reports in the literature that documented sporadic bilateral projections from the cortex to the contralateral thalamus, particularly from the hippocampus (Mathiasen et al. 2019), prefrontal cortex (Vertes 2002; Szczupak, Iack, et al. 2021), and primary motor cortex (Hoerder-Suabedissen et al. 2018; Szczupak, Iack, et al. 2021). This suggests that TCs may represent a normotypical pathway for interhemispheric connectivity and could be present in other mammals.

In our previous work, we also found that corpus callosum dysgenesis (CCD), a developmental callosal malformation, altered the TC's anatomical presentation and tissue properties (e.g. fractional anisotropy [FA]) (Szczupak, Iack, et al. 2021). Developmental malformations can generally result in anatomical alterations that disrupt the brain's wiring. For example, CCD can lead to atypical anatomical white matter rewiring, such as the Probst bundle (Probst 1901), sigmoid bundle (Tovar-Moll et al. 2006; Paul et al. 2007; Kasprian et al. 2013), and intercortical bundle (Tovar-Moll et al. 2014). Furthermore, these alterations lead to global network changes in human subjects (Owen et al. 2013; Jakab et al. 2015; Siffredi et al. 2021; Szczupak, Kossmann Ferraz, et al. 2021) and have also been observed in nonhuman primates (NHPs; Szczupak, Yen, et al. 2020) and mice (Edwards et al. 2020; Szczupak et al. 2020; Rayêe et al. 2021).

Received: June 15, 2023. **Revised:** October 2, 2023. **Accepted:** October 3, 2023

In this study, we sought to probe the existence of TCs in primates. We employed high-resolution diffusion imaging, viral axonal tracing, and fMRI techniques to investigate the TCs in 3 NHP species and comprehensively describe their macroscopic anatomy, fine axonal connectivity, development, and function. Furthermore, to extend the scope of our findings, we applied diffusion-weighted imaging to examine the presence of TCs in humans in both healthy human subjects and patients with brain malformations.

Materials and methods

Animals

All procedures in this study were approved by the Animal Care and Use Committee of the National Institute of Neurological Disorders and Stroke (IACUC protocol #1261-18). The marmosets in this study were socially housed with a minimum of 2 animals per cage. The animals were fed an ad libitum diet and had unrestricted access to water. The marmosets were also provided with toys and other environmental enrichment.

The marmosets used for resting-state fMRI (rsfMRI) were trained for awake fMRI scans (Silva et al. 2011). Anatomical flexible helmets were designed to fit the animal's head perfectly and to provide robust and comfortable support to minimize head motions during acquisition. In addition, the animal's face was monitored with an infrared camera during scans to ensure that the animal was awake and comfortable throughout the session.

Ex vivo diffusion-weighted MRI

All MRI images were acquired using the 9.4T Bruker biospin scanner at the University of Pittsburgh Neurobiology Department and using the 11.7 vertical scanner Bruker biospin at the University of Pittsburgh Animal Imaging Center.

Adult marmosets

The brains of 3 adult common marmosets (*Callithrix jacchus*) were gadolinium doped (0.02%) (Liu et al. 2020), placed in a custom-designed, 3D-printed holder, and inserted in a 30-mm falcon tube containing Fomblin. Diffusion-weighted images were acquired using an 11.7T/89-mm vertical bore MRI system equipped with a Micro2.5 gradient set of 1,500 mT/m and a 30-mm quadrature coil. Diffusion-weighted 3D spin-echo EPI images were acquired using the following parameters: TR/TE = 200/30 ms, $\delta/\Delta = 2.6/5.6$ ms, field of view = 35.5 × 25 × 22 mm, matrix = 444 × 312 × 275, yielding an isotropic resolution of 80 μm; number of averages = 1; 240 diffusion-weighting directions split in 3 shells of 31, 57, and 127 directions; *b*-values = 1,000, 1,500, and 2,400 s/mm^2 with 25 *b*0 images.

Neonate marmosets

The brains of 2 neonate common marmosets (*C. jacchus*) were gadolinium doped (0.02%) (Liu et al. 2020) and were placed in a custom-designed, 3D-printed holder containing Fomblin. Diffusion-weighted images were acquired using a 9.4T horizontal bore small animal MRI system equipped with a custom-made 17-cm gradient (Resonance Research Inc, Billerica, MA), performing at 450 mT/m gradient strength, and with a custom-made 30-mm millipede quadrature coil. Diffusion-weighted 3D spin-echo EPI images were acquired using the following parameters: TR/TE = 350/42 ms, $\delta/\Delta = 6/14$ ms, field of view = 24 × 18 × 16 mm, matrix = 300 × 225 × 200, yielding an isotropic resolution of 80 μm; number of averages = 1; bandwidth = 300 kHz; 90 diffusion-weighting directions split in 2 shells of 30 and 90 directions; *b*-values = 1,500, 3,000 s/mm^2 with 4 *b*0 images.

Cebus

The brain of a capuchin monkey (*Cebus apella*) was placed in a custom-designed, 3D-printed holder containing Fomblin. Diffusion-weighted images were acquired using a 9.4T horizontal bore small animal MRI system equipped with a custom-made 17-cm gradient (Resonance Research Inc), performing at 450 mT/m gradient strength, and with an 86 mm coil. Diffusion-weighted 3D spin-echo EPI images were acquired using the following parameters: TR/TE = 250/50 ms, $\delta/\Delta = 6/14$ ms, field of view = 48 × 28 × 28 mm, matrix = 240 × 140 × 140 mm, yielding an isotropic resolution of 200 μm; number of averages = 1; bandwidth = 300 kHz; 30 diffusion-weighting directions; *b*-values = 1,500 s/mm^2; and 60 *b*-values = 3,000 s/mm^2 with 4 *b*0 images.

Macaque

The brain of a rhesus macaque (*Macaca mulatta*) was placed in a custom-designed, 3D-printed holder containing Fomblin. Diffusion-weighted images were acquired using a 9.4T horizontal bore small animal MRI system equipped with a Bruker BGA20 gradient, performing at 300 mT/m gradient strength, equipped with an 86-mm coil. Diffusion-weighted 3D spin-echo EPI images were acquired using the following parameters: TR/TE = 200/31 ms, $\delta/\Delta = 8/16$ ms, field of view = 65 × 55 × 71 mm, matrix = 325 × 275 × 355, yielding an isotropic resolution of 200 μm; number of averages = 1; bandwidth = 300 kHz; 30 diffusion-weighting directions; *b*-values = 1,500 s/mm^2; and 30 *b*-values = 3,000 s/mm^2 with 4 *b*0 images.

Adult mice

The brains of 6 adult C57bl6/J mice were gadolinium doped (0.02%) (Szczupak et al. 2020), placed in a custom-designed, 3D-printed holder, and inserted in a 15-mm falcon tube containing Fomblin. Diffusion-weighted images were acquired using a 11.7T/89 mm vertical bore MRI system equipped with a Micro2.5 gradient set of 1,500 mT/m and with a 15-mm quadrature coil. Diffusion-weighted 3D spin-echo EPI images were acquired using the following parameters: TR/TE = 350/28 ms, $\delta/\Delta = 2.6/5.6$ ms, field of view = 15.36 × 11.52 × 7.68 mm, matrix = 192 × 144 × 96, yielding an isotropic resolution of 80 μm; number of averages = 1, 240 diffusion-weighting directions split in 2 shells of 30 and 90 directions; *b*-values = 1,500 and 3,000 s/mm^2 with 25 *b*0 images.

Neonate mice

The brains of 4 neonate C57bl6/J mice were placed in a custom-designed, 3D-printed holder and were inserted in a 10-mm falcon tube containing Fomblin. Diffusion-weighted images were acquired using an 11.7T/89 mm vertical bore MRI system equipped with a Micro2.5 gradient set of 1,500 mT/m and with a 10-mm quadrature coil. Diffusion-weighted 3D spin-echo EPI images were acquired using the following parameters: TR/TE = 1500/38 ms, $\delta/\Delta = 2.6/5.6$ ms, field of view = 15 × 9.6 × 9.6 mm, matrix = 300 × 192 × 192, yielding an isotropic resolution of 50 μm; number of averages = 1; 90 diffusion-weighting directions split in 2 shells of 30 and 60 directions; *b*-values = 1,500 and 3,000 s/mm^2 with 4 *b*0 images.

T_2^* anatomical images

The ultrahigh-resolution T_2^* image of a common marmoset brain was previously published by Schaeffer et al. (2022) and is briefly

described here. The brain was gadolinium doped (0.02%) and was placed in a custom-designed, 3D-printed holder containing Fomblin. Flash images were acquired using a 9.4T horizontal bore small animal MRI system equipped with a custom-made 17 cm gradient (Resonance Research Inc), performing at 450 mT/m gradient strength, and with a custom-made 30-mm coil millipede quadrature coil. 3D gradient-echo images were acquired using the following parameters: TR/TE = 100/12 ms, FOV = 35 × 25 × 22 mm, matrix = 1,400 × 1,000 × 870, yielding an isotropic resolution of 25 μm; number of averages = 1; bandwidth = 50 kHz; flip angle = 50.6 (optimized for earns angle at a measured T1 = 220 ms).

In vivo diffusion-weighted MRI

Marmosets

Multishell diffusion MRI data were previously published by Liu et al. (2021) and are briefly described here. Data were collected using a 7T Bruker scanner with a 2D diffusion-weighted spin-echo EPI sequence: TR = 5.1 s, TE = 38 ms, FOV = 36 × 28 mm, matrix size = 72 × 56, slice thickness = 0.5 mm, a total of 400 DWI images for 2-phase encodings (blip-up and blip-down), and each has 3 b-values (8 $b = 0$ s/mm^2, 64 $b = 2{,}400$ s/mm^2, and 128 $b = 4{,}800$ s/mm^2).

Human ultraresolution data

The human neurotypical in vivo ultra-resolution data were previously published by Wang et al. 2021 and are briefly described here. Data were acquired from a single subject across 18 scans with a spatial resolution of 0.76 mm in 2,808 directions, which were split into 2 different shells (840 $b = 1{,}000$ s/mm^2 and 1,680 $b = 2{,}500$ s/mm^2 and 288 et al. = 0 s/mm^2) to ensure accurate shell sampling and SNR at this resolution.

Human CCD subjects

Data from CCD patients were acquired using a Prisma scanner following the Human connectome project protocol (HCP), previously published by Szczupak, Kossmann Ferraz, et al. (2021) and briefly described here. Four CCD patients (2 males and 2 females, age mean = 18, SD = 6.36) were recruited by D'or Institute (Rio de Janeiro, Brazil). Images were acquired following the HCP criteria for 3.0 Tesla scanners. The diffusion scheme of 200 directions was split into 2 different shells with b-values of 1,500 and 3,000 s/mm^2, with a 1.5-mm isotropic resolution acquired in 2 different phase encoding directions, to minimize the drop-out signal. IDOR's Institutional Ethics Committee approved experiments under protocol # 44421415.2.0000.5249.

Infant human subjects

MR imaging were performed in 2 infants with non-CCD brain malformations. The first patient, age 16 months, presented enlarged ventricles (Fig. 6G–L), achondroplasia, and abnormal gyration in temporal lobes. The second patient, 10 weeks-old (Fig. 6A–F) presented bilateral frontal and perisylvian polymicrogyria in clinically indicated examinations on a 1.5 T MR system (Siemens Aera) using a head coil. Sedation was used only for the 16-month-old individual, while the 10-week-old infant was imaged without anesthesia. Whole-brain echo-planar diffusion tensor axial images were acquired using 30 gradient-encoding directions, TE = 135 ms, TR = 10,900 ms, Grappa acceleration factor = 2, b-values = 0 and 700 s/mm^2 and were reconstructed to an asymmetric voxel size of 1.57 × 1.57 × 2 mm. Experiments were approved by the Medical University of Vienna's Institutional Ethics Committee under protocol #1604/2018.

Image denoising

Human images were denoised using Mrtrix 3.0 (Tournier et al. 2019), while the animal images were denoised using the variance stabilization transformation (VST) approach. The noise on the magnitude image is known to follow a Rician distribution (Foi 2011; Aja-Fernández and Vegas-Sánchez-Ferrero 2016). Therefore, we applied the forward VST to stabilize the noise variance and convert the signal-dependent noise into signal-independent noise with a Gaussian-like distribution. Then, the block-matching and 4D filtering (a nonlocal transform-domain filter designed for volumetric data corrupted with Gaussian signal-independent noise) algorithm was applied to denoise the images in the VST domain (Maggioni et al. 2013). Finally, the inverse VST was used to take the data back to their original magnitude space. We emphasize that this approach is particularly advantageous to high-resolution images (Santini et al. 2021), making it a perfect fit for our high-resolution animal data.

Diffusion imaging processing

All diffusion images were corrected for eddy current-induced geometric distortions using FSL 6.0 software (Andersson and Sotiropoulos 2016), and the human images were denoised using Mrtrix 3.0 software (Tournier et al. 2012). The diffusion tensor model was fitted to the data, visualized, and quantified in DSI Studio 2023 software (Yeh 2020). FA values were compared with the nonparametric Kruska-Wallis test.

Functional MRI

fMRI data were previously published by Schaeffer et al. (2022), and the correlations were obtained through marmosetbrainconnectome.org, which is a freely and publicly available resource (https://marmosetbrainconnectome.org). This database contains rsfMRI data from 31 awake marmosets (*C. jacchus*, 8 females; age: 14–115 months; weight: 240–625 g) that were acquired from the National Institutes of Health (26 animals) and from the University of Western Ontario (5 animals). Briefly, NIH images were acquired with the following protocol TR = 2,000 ms, TE = 22.2 ms, flip angle = 70.4°, field of view = 28 × 36 mm, matrix size = 56 × 72, voxel size = 0.5 × 0.5 × 0.5 mm, slices = 38, bandwidth = 134 kHz, GRAPPA acceleration factor: 2 (left–right), while the images from the University of Western Ontario were acquired with the following protocol TR = 1,500 ms, TE = 15 ms, flip angle = 35°, field of view = 64 × 64 mm, matrix size = 128 × 128, voxel size = 0.5 × 0.5 × 0.5 mm, slices = 42, bandwidth = 500 kHz, GRAPPA acceleration factor: 2 (anterior–posterior).

Viral injection and histology

For neuronal tract tracing, a 2 μL solution containing 2 × 10^{11} copies/μL of AAV9 (AAV9-hSyn-mCherry, Penn Vector Core, University of Pennsylvania) was loaded into a 5-μL Hamilton syringe that was mounted to the arm of a stereotaxic frame (Stoelting Instruments), and it injected into the dorsolateral prefrontal cortex (A6DR) of an adult marmoset. The stereotaxic coordinates were obtained from the MBM atlas (Liu et al. 2018). These specific brain regions were chosen because they are known to make corticothalamic interhemispheric connections in different mammalian species (Vertes 2002; Szczupak, Iack, et al. 2021). Four weeks after the injection, the animals were euthanized and perfused with PBS 0.1 M followed by PFA 4% in PBS, and their brains were extracted and were placed in 30% sucrose in 0.1 M PBS for cryoprotection for a week. The brains were coronally sliced into 60-μm sections, mounted, and sealed in histological slides.

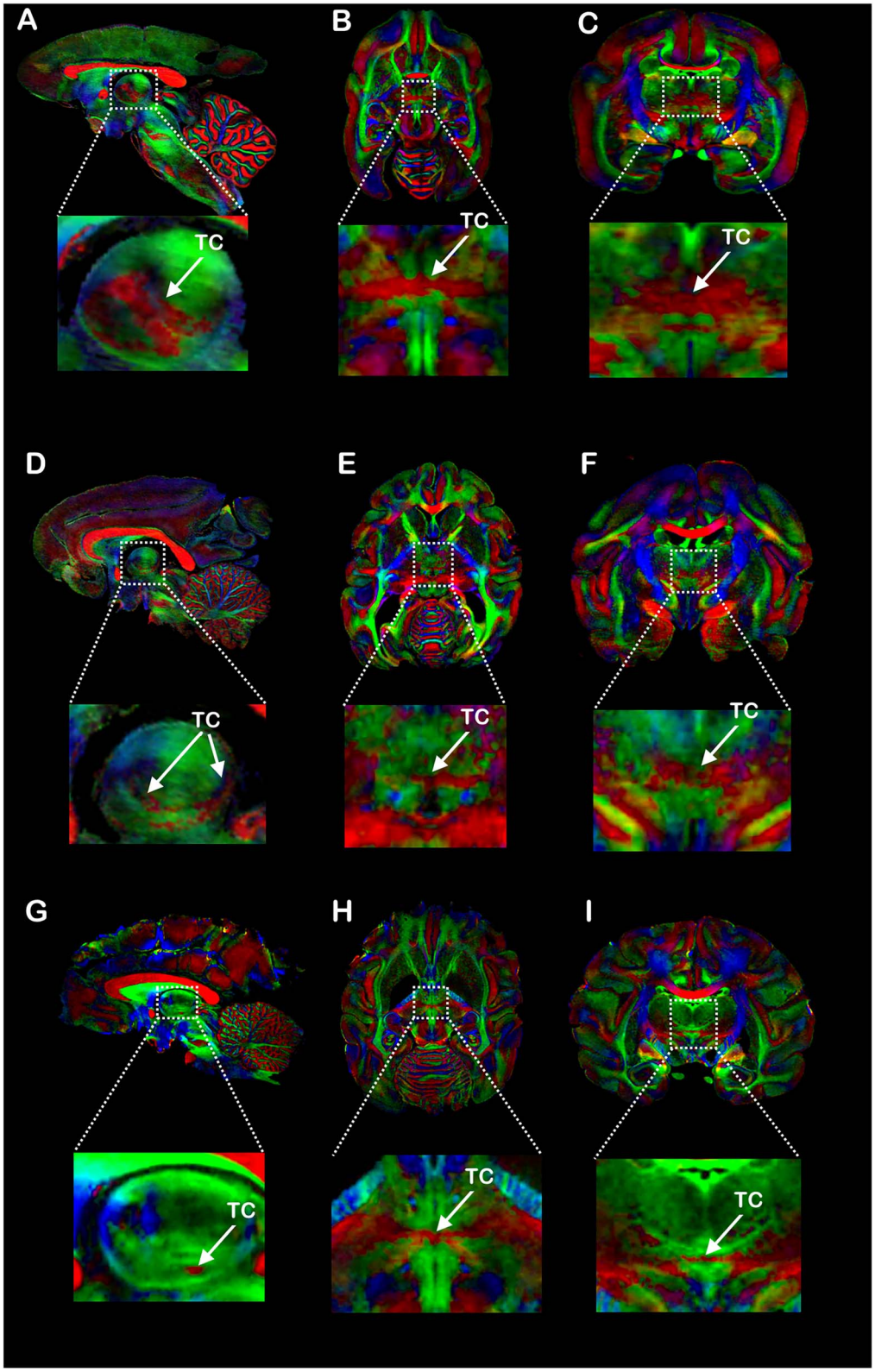

Fig. 1. NHP comparative TCs. Diffusion-encoded colormap (DEC) images of FA of midsagittal, axial, and coronal brain slices of 3 different NHP species: A–C) marmoset, D–F) capuchin, and G–I) macaque. Insets show the presence of white matter fibers traversing the midline at the thalamus, suggesting the presence of TCs (arrows). In the DEC images, red represents the mediolateral (ML), green represents the AP, and blue represents the dorsoventral (DV) directions.

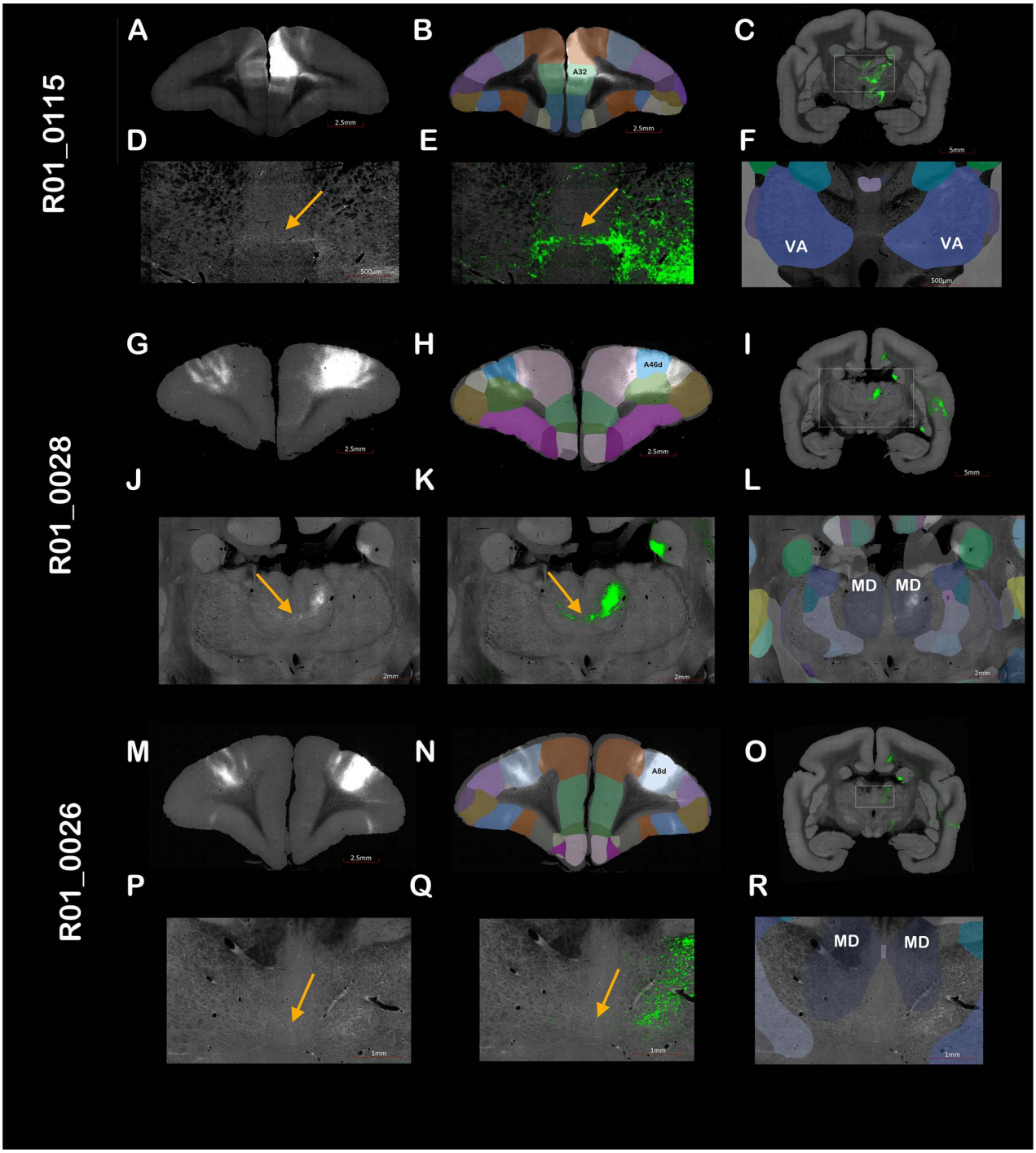

Fig. 2. TCs axonal tracing in the marmoset brain. Coronal view of 3 different experiments from the Brain/Minds Marmoset PFC Tracer Connectome project depicting the anterograde AAV-9 tracers injection site in A) A32, G) A46d, and M) A8d overlayed with the B, H, and N) Riken atlas parcellation. Cortical projections from the injection site to the contralateral thalamus via the TCs can be seen in (C), (I), and (O) and zoomed in (D), (J), and (P) (pointed by arrows). Axons were highlighted using the E, K, and Q) automatic Brain/Minds viewer, and the F, L, and R) atlas were overlayed.

Images were acquired using an AxioVision (Carl Zeiss Microimaging) microscope with a 10× objective lens.

Results

TCs in the NHP brain

We imaged the brains of 3 different NHP species ex vivo with high-resolution DWI to look for TCs (Fig. 1). We identified white matter tracts traversing the thalamus at the midline in all 3 monkey brains, suggesting that TCs are a common feature of the primate brain. These TCs showed different presentations. In the marmoset, the TCs were primarily oriented diagonally along the anteroposterior (AP) axis and were segmented into different elongated patches (Fig. 1A–C). In the capuchin brain, the TCs were dispersed in a lemniscal fashion and were split into 2 curved but parallel pathways along the inferior portions of the thalamus (Fig. 1D–F). In the rhesus macaque, we identified several patches of white matter fibers traversing the thalamus Fig. 1G–I). We

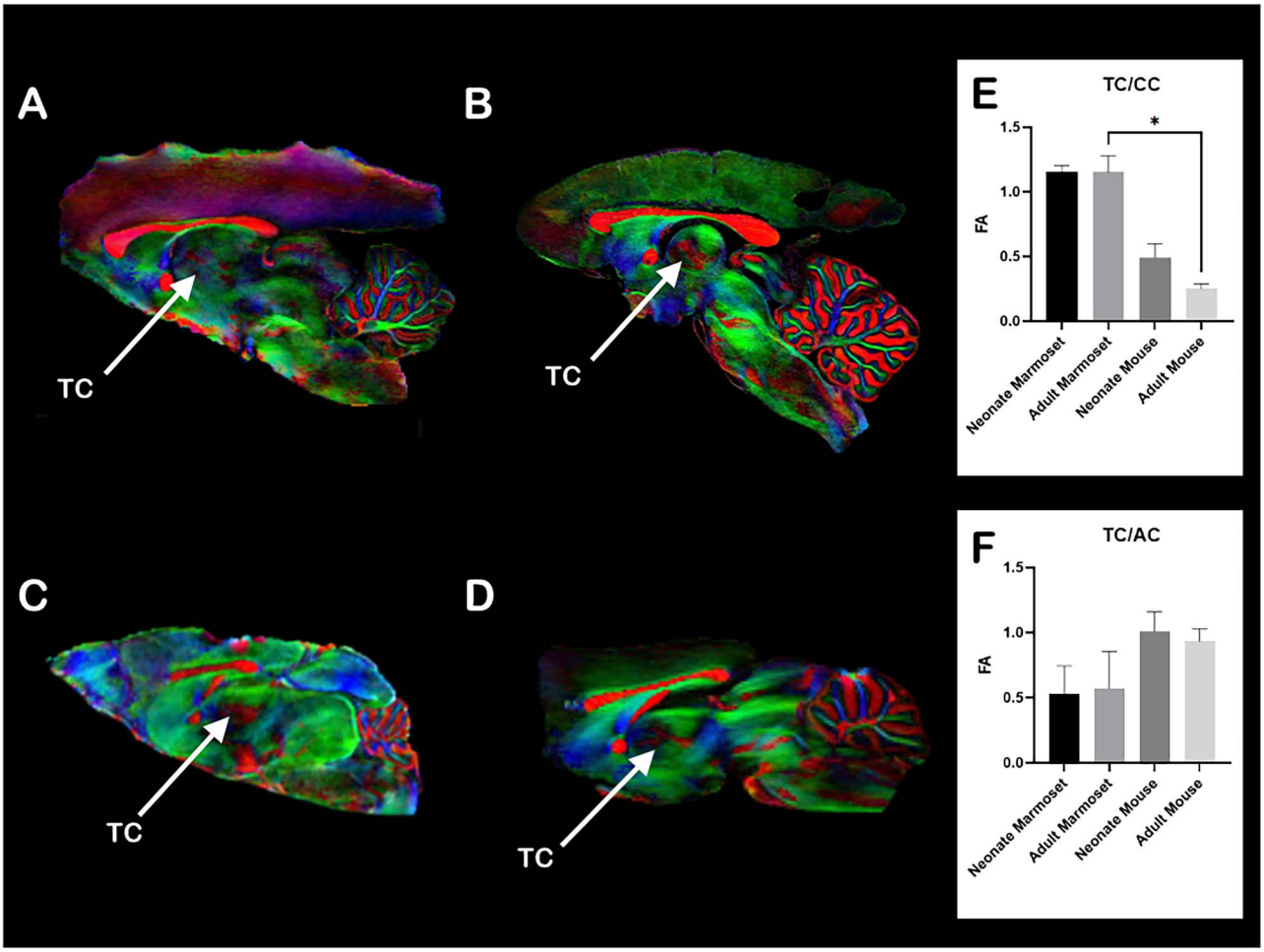

Fig. 3. TCs' development. Direction-encoded diffusion-weighted images show the brain of a A) neonate and B) an adult marmoset and C) a neonate and D) adult mouse FA maps with the TCs indicated by the arrows. E) A plot of the FA values of the TCs normalized by the genu of the CC and F) the anterior commissure (AC). In the direction-encoded colormaps, red represents ML diffusion, green represents AP diffusion, and blue represents DV diffusion. ∗*P*-value = 0.0187.

also identified TCs in marmosets in DWI scans acquired in vivo (Supplementary Fig. 1) and in ultra-high-resolution ex vivo T2∗ images (Supplementary Fig. 2). These MRI modalities establish the presence of white matter fibers traversing the midline at the thalamus, allowing further investigation of the TCs.

TC axonal tracing in the marmoset brain

To validate the DWI results shown in Fig. 1, we used the new prefrontal cortex viral axonal tracing Brain/Minds resource (Watakabe et al. 2023) to show the injection of 3 marmoset brains with AAV9 anterograde tracer in 3 distinct brain regions. In the first animal (experiment number R01_0115), the viral tracer was injected centered into A32 (Fig. 2A and B). This injection shows clear communication to the contralateral thalamus via the TCs through the ventral anterior thalamic nuclei (Fig. 2C–F). The second animal (experiment number R01_0028) was injected centered in the area A46d (Fig. 2G and H), showing projections from the cortex to the contralateral thalamus via the TCs crossing the midline at the level of the mediodorsal (MD) nuclei (Fig. 2I–L). The third animal (experiment number R01_0026) was injected centered into A8d (Fig. 2M and N), showing diffuse connectivity from the cortex to the contralateral thalamus via the TCs dorsal to the MDs (Fig. 2O–R). Furthermore, we have injected a marmoset at the dorsolateral prefrontal cortex (Supplementary Fig. 3). Our data clearly show cohesive white matter fiber bundles crossing the midline via the CC (Supplementary Fig. 3B), and diffuse fibers traversing the midline via the TC (Supplementary Fig. 3C and D). Moreover, we compared this dataset with a histology slide stained with luxol fast blue that shows myelinated axonal fibers crossing the thalamic midline (Supplementary Fig. 4).

TCs' normal development

We employed high-resolution ex vivo DWI to investigate the TCs' development in marmosets and mice by scanning the brains of neonate (p0, Fig. 3A and C) and adult (Fig. 3B and D) animals. We could clearly resolve TCs at both ages, suggesting TCs are present at the early developmental stages. To prevent confounding factors related to the MRI scanner, diffusion scheme, sequence differences, or interspecific differences, we compared the ratio of FA of the TCs with other well-studied commissures (CC and AC). In both species, we found no statistical differences in the FA ratio between neonates and adults (Fig. 3E and F). However, marmosets presented a higher TC/CC ratio than mice ($P = 0.0187$—Fig. 3E), likely due to the CC differences in FA between marmosets and mice.

TC functional connectivity

To further evaluate the connectivity of brain areas with the contralateral thalamus, we investigated the functional connectivity

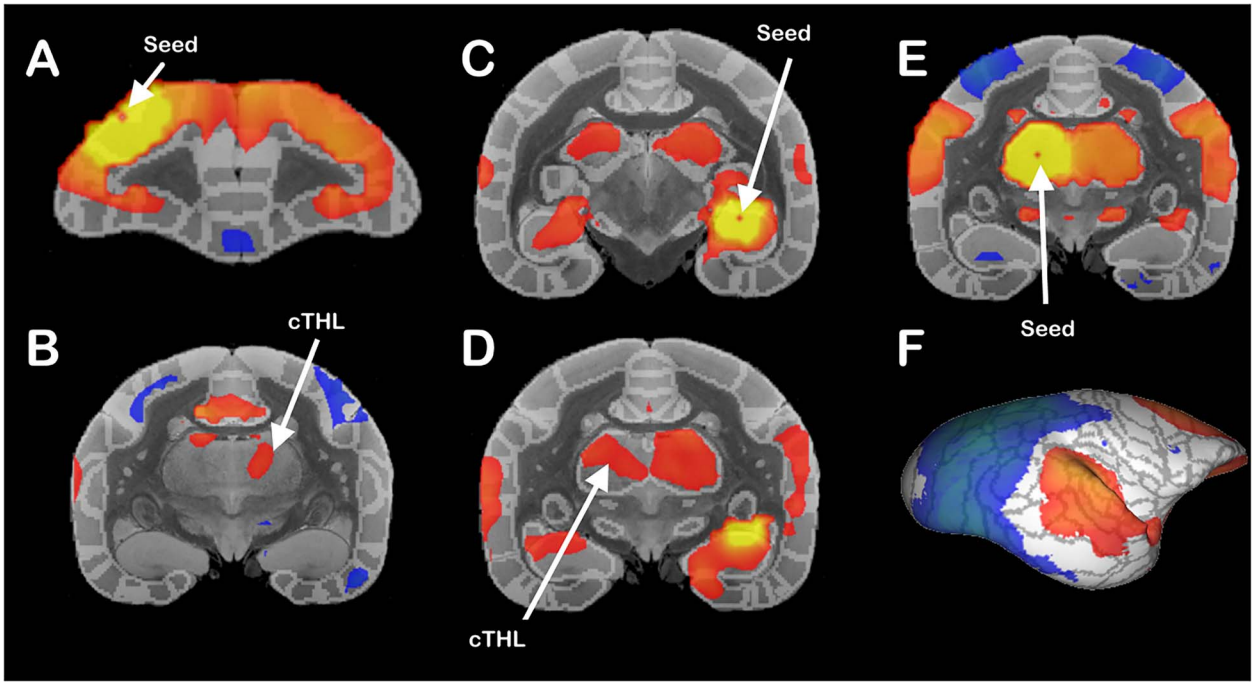

Fig. 4. Marmoset functional connectivity. Functional resting-state connectivity averaged populational correlation map of 31 marmosets reveals cortical functional connectivity with the contralateral thalamus. We used single-voxel seeds (arrows) in the A) dorsolateral prefrontal cortex (A6DR) and C) dorsal hippocampus and showed that both areas are functionally connected to the contralateral thalamus (cTHL) (B and D, respectively). E) Thalamic seed and F) contralateral cortical functional connectivity across the whole hemisphere.

in the populational averaged map of 31 adult marmosets (Schaeffer et al. 2022). We analyzed the connectivity of a seed voxel within the dorsolateral prefrontal cortex (A6DR, Fig. 4A) and the hippocampus (Fig. 4C) and verified that both of these regions were positively correlated to the contralateral thalamus (Fig. 4B and D), indicating functional interhemispheric connectivity. Conversely, we placed a seed in the thalamus (Fig. 4E) and observed both positive and negative correlations with cortical regions in the contralateral hemisphere (Fig. 4F). The thalamic connectivity spreads throughout the contralateral hemisphere, posing the TCs as an essential connectivity hub across hemispheres. Different cortical seeds revealed different thalamic contralateral activation depending on the placement of the cortical seed, indicating a TC topographical relationship (Supplementary Fig. 5).

Human TCs

In addition to identifying the TCs in the NHP brain, we investigated their presence in the human brain. In a super-resolution DWI scan of a healthy subject, we could not identify any evidence of TCs in the sagittal, coronal, or axial views (Fig. 5A–F). However, a callosal dysgenesis (CCD) patient clearly showed a TC (Fig. 5G–L). In a cohort of 11 CCD patients, we identified TCs in 4 subjects (Supplementary Fig. 6). We also identified TCs in 2 infants from an Austrian patient cohort with non-CCD brain malformations (Fig. 6), indicating that the TCs may be associated with many different brain malformations. Our data show that, while not normally discernible in the healthy human brain, TCs can form in subjects afflicted with developmental disorders, posing the TCs as an alternative pathway for interhemispheric communication in primates.

Discussion

In this work, we leverage high-resolution diffusion-weighted imaging, viral axonal fiber tracking, and fMRI to accurately describe and characterize the TCs in the primate brain at birth and adulthood. We verified the existence of TCs in 3 NHP species and humans with developmental callosal malformations. We found that the TCs are present in the neonate brain, suggesting their morphogenesis follows the primary commissural system. Furthermore, we described how the TCs contribute to a clear functional connectivity of the thalamus with the contralateral cortex. Altogether, our findings pose the TCs as a common interhemispheric pathway in the callosal mammalian brain.

TCs in the NHP brain

It is necessary to distinguish the TCs from the interthalamic adherence, an anatomical structure of gray and white matter defined by the union between the hemispheric sides of the thalamus at the midline. Here, we refer to TCs as organized white matter fiber bundles connecting the cortex to the contralateral thalamus.

It is also important to note that the finding of cortical projections to the contralateral thalamus is not novel. The literature offers several reports of sporadic bilateral cortico-thalamic projections in different species (Molinari et al. 1985; Vertes 2002; Hoerder-Suabedissen et al. 2018; Mathiasen et al. 2019; Halassa 2022), with recent work suggesting these findings being more general than previously thought (Szczupak, Iack, et al. 2021; Parra et al. 2022; Şahin et al. 2023). Here, we show that these interhemispheric projections connecting the cortex to the contralateral thalamus form an organized commissural system that contrasts the sporadic interhemispheric projections previously reported. Technical limitations in performing axonal tracing and the unavailability of high-resolution diffusion-weighted imaging likely precluded more detailed investigations of the interhemispheric brain connectivity.

In previous work, we identified the TCs in C57BL6 and Balb/c mice (Szczupak, Iack, et al. 2021). The TCs in the C57BL6 mouse brain presented a stereotypical anatomical formation with

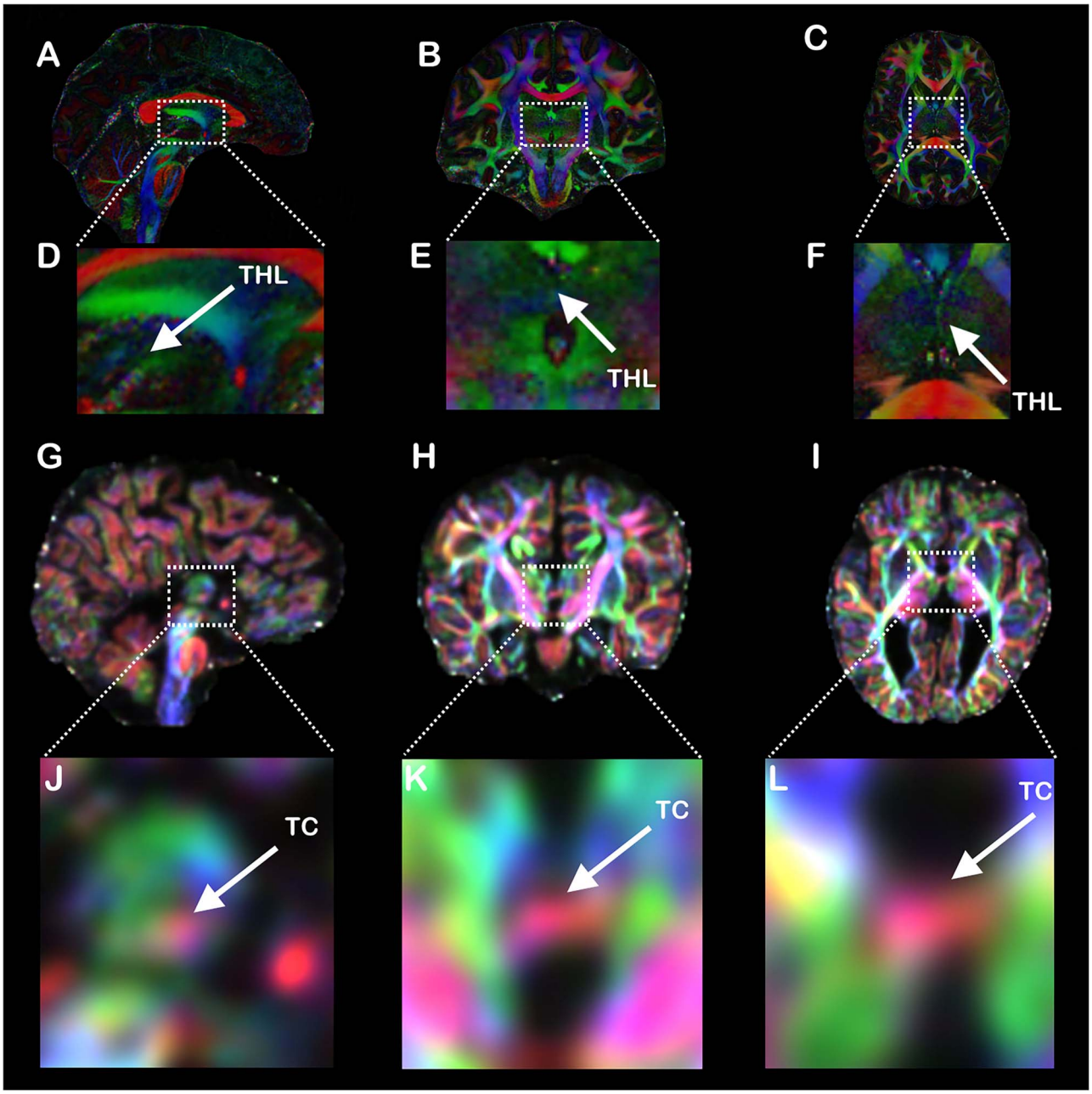

Fig. 5. Human TCs. Direction-encoded colormaps of diffusion-weighted FA showing the thalamic region of a healthy human subject in A) sagittal, B) coronal, and C) axial views. No visible TCs were detected in the D–F) zoomed insets. Equivalent brain views of a patient with G–I) CCD showing a clear TC on the J–l) insets. In the direction-encoded colormaps, red represents ML diffusion, green represents AP diffusion, and blue represents DV diffusion.

4 distinct patches distributed along the AP axis of the thalamus. Here, we confirmed that TCs also exist in the brains of 3 NHP species. However, unlike rodents, the anatomical organization of the TCs along the thalamic midline varied substantially across the 3 species. Marmosets presented a clear and well-organized TC composed of different elongated patches distributed diagonally along the thalamus, while the capuchin monkey's TCs spread along 2 ribbon-like patterns, and the macaque showed a broader dispersal of TCs.

Although the TC is a central commissure connecting the brain hemispheres, it is distinct from the large AC of metatherian mammals, such as marsupials (Suárez et al. 2018), which connects both cortical hemispheres in the absence of the CC. It remains to be shown whether TCs are also featured in the brains of marsupials.

Axonal connectivity

Due to their sparse nature, diffuse connectivity pattern, and inherently low FA, it is challenging to map the axonal projections crossing the thalamic midline via the TCs with histology or diffusion-weighted imaging. We used AAV-9 anterograde neuronal tracers to verify the results shown with diffusion-weighted imaging and found several areas of the marmoset prefrontal cortex projecting to the contralateral thalamus via TCs. Similar connectivity was found in the frontal areas of the mouse cortex (Vertes 2002; Szczupak et al. 2021). A32 and A46d have more dense and compact TC projections, while A8d and A6DR have more diffuse interhemispheric communication to the contralateral hemisphere. The dorsolateral prefrontal cortex is a central hub of the default-mode network (DMN) (Liu et al. 2019); therefore,

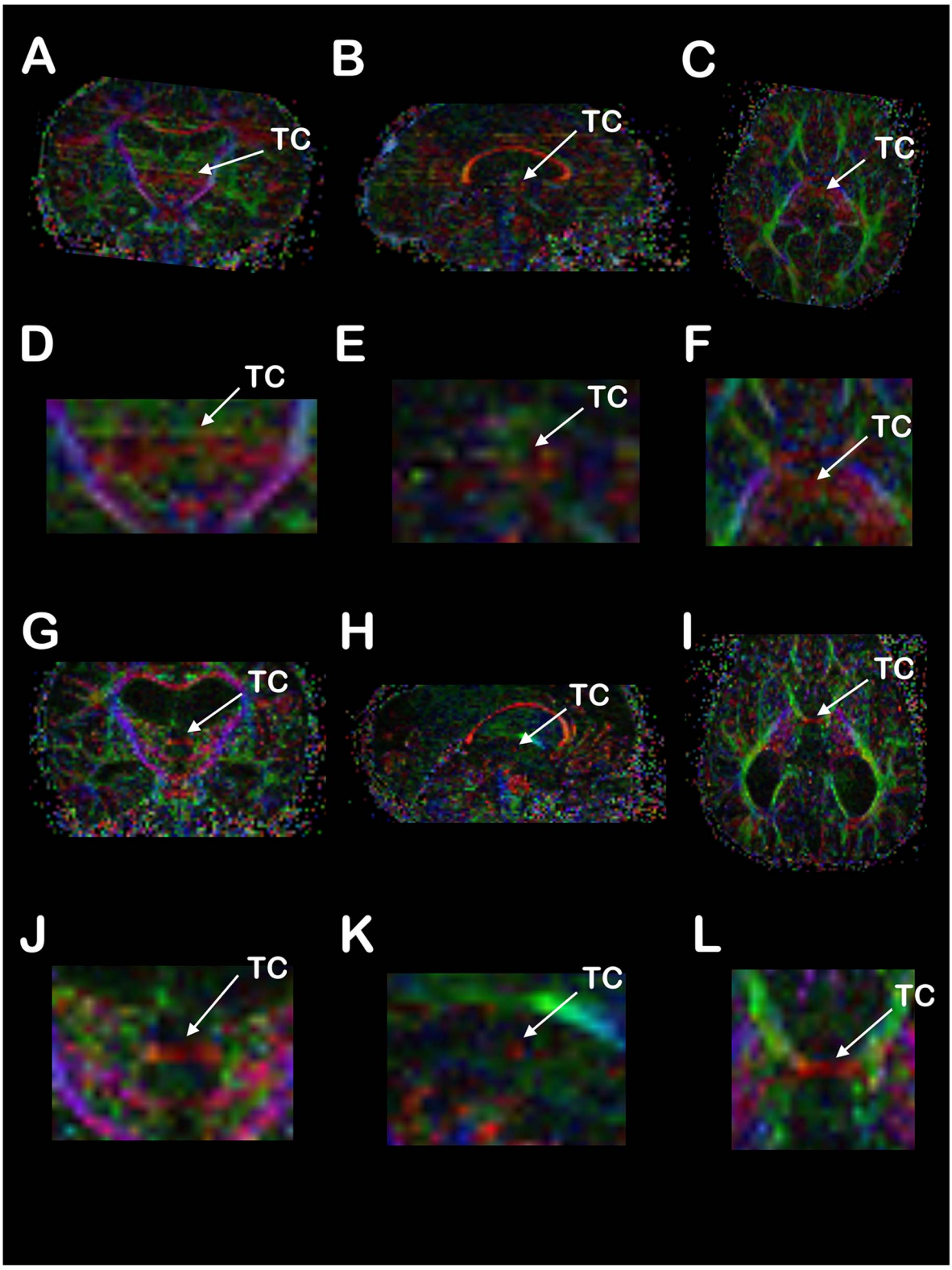

Fig. 6. Human infant TCs. Direction-encoded colormaps in A, G) coronal, B, H) sagittal, and C, I) axial views of diffusion-weighted FA showing the thalamic region of 2 infants (A–F and G–L) with brain malformations. Visible TCs were detected on the zoomed insets (D–F and J–L). In the direction-encoded colormaps, red represents ML diffusion, green represents AP diffusion, and blue represents DV diffusion.

it is reasonable to link these commissures with the DMN and its interhemispheric synchrony.

Development

It is well documented that white matter fiber bundles change along development through life into aging. Although most fibers are developed during the gestational period, myelination (Gibson et al. 2014), pruning (LaMantia and Rakic 1994), and fine dendritic morphology (Bahia et al. 2018) are plastic and vary longitudinally. Our work investigated brain changes with MRI across species and ages. Therefore, we compared the TCs' FA normalized by the AC and CC FA to avoid confounding effects from the difference in pulse sequences or MRI scanners and hardware (Pomponio et al. 2020). We have found no differences between neonates and adults in both marmosets and mice, indicating that the TCs have a similar development as the CC and AC and are likely regulated by similar processes. However, we have found a statistically significant difference between the marmoset adult TC/CC ratio relative to adult mice, but no difference in TC/AC ratio. Therefore, this is likely due to differences in the CC FA between species. This increase in CC FA agrees with a larger cortical volume in primates relative to rodents (Rakic 2009).

Functional connectivity

After investigating the structural connectivity of the TCs in the NHP brain, we analyzed the functional connectivity of the marmoset brain to understand whether these axonal fibers that cross the midline via the TC can functionally connect brain areas. Our data (shown in Supplementary Fig. 5) demonstrate a clear topographical relationship between the cortical areas and the contralateral thalamus, suggesting that the TCs contribute to whole-brain functional connectivity (which includes both monosynaptic and polysynaptic connections (Hori et al. 2020). Furthermore, our findings indicate that the thalamus mediates not only ipsilateral (Sherman 2016) but also contralateral cortical connectivity. Figure 7 shows 1 possible model for how the monosynaptic TC connections can influence the whole-brain functional connectivity: The thalamus receives contralateral cortical information via the TCs (Fig. 7, blue), which activates ipsilateral thalamocortical projections (Fig. 7, purple) that facilitate or inhibit cortical regions receiving contralateral cortical information via other commissures (Fig. 7, magenta). Therefore, the thalamus is a control hub that mediates the cortico-cortical interhemispheric connectivity and synchrony (Fig. 7).

Human TC

We used an ultra-high-resolution diffusion image to investigate the presence of the TCs in the healthy human brain. We could not find white matter fibers crossing the midline via the thalamus, an expected finding, given most human thalami are anatomically separated. However, we identified the TCs in half of the CCD cohort (with a higher prevalence of fused thalami) and in the 2 Austrian infants with brain malformations. We hypothesize that the molecular and cellular substrates to the development of TCs are present in the healthy human brain, but only develop in brain malformations, likely due to changes in the overall midline anatomy. When the brain has a developmental malformation, TCs can form naturally and work as a backup system to integrate the hemispheres in the human brain.

It is important to notice that we detected the TCs in 2 patients of the Brazilian cohort and both Austrian patients without thalamic adherences or other crossing fibers or additional gray matter that could be a confounding effect.

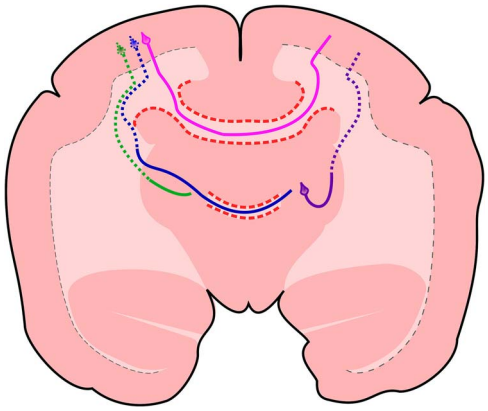

Fig. 7. Schematic figure portraying the TCs in a marmoset brain. Coronal view of a marmoset brain showing the CC in magenta, intrahemispheric ipsilateral cortico-thalamic communication in green, intrahemispheric contralateral cortico-thalamic communication in purple, and the TCs in blue. This circuit allows the thalamus to communicate with its own hemisphere and to play a role in the interhemispheric cortical connectivity.

Future studies shall investigate the presence of the TCs in the human brain in different biological contexts, their functional relevance, and how the TCs are affected by various diseases.

Acknowledgments

We thank the International Research Consortium for the Corpus Callosum and Cerebral Connectivity (IRC5, https://www.irc5.org) members and affiliates for discussions and input. We also thank Professor Kim Phillips, Chair of the Department of Neuroscience at Trinity University, for providing the *C. apella* brain tissue. The authors also thank Dr. T. Kevin Hitchens of the Advanced Imaging Center at the University of Pittsburgh for collecting the *ex vivo* diffusion-weighted imaging data for the Adult Marmosets, Adult Mice, and Neonate Mice.

Authors' contributions

Diego Szczupak (Conceptualization, Data curation, Formal analysis, Investigation, Methodology, Resources, Validation, Visualization, Writing—original draft, Writing—review & editing), David J. Schaeffer (Formal analysis, Investigation, Methodology, Resources, Writing—review & editing), Xiaoguang Tian (Formal analysis, Writing—review & editing), Sang-Ho Choi (Data curation, Investigation, Methodology, Writing—review & editing), Fang-Cheng (Software, Writing—review & editing), Pamela Meneses Iack (Formal analysis, Writing—review & editing), Vinicius P. Campos (Software, Writing—review & editing), J. Patrick Mayo (Resources, Writing—review & editing), Janina Patsch (Data curation, Investigation), Christian Mitter (Investigation, Writing—review & editing), Amit Haboosheh (Data curation, Formal analysis), Ha Seung Kwon (Data curation, Resources), Marcelo A.C. Vieira (Software, Writing—review & editing), Daniel S. Reich (Funding acquisition, Resources, Writing—review & editing), Steve Jacobson (Data curation, Funding acquisition, Writing—review & editing), Gregor Kasprian (Funding acquisition, Investigation, Resources, Writing—review & editing), Fernanda Tovar-Moll (Conceptualization, Funding acquisition, Investigation, Project administration, Resources, Supervision, Writing—review & editing), Roberto Lent (Conceptualization, Investigation, Writing—review & editing), and Afonso C. Silva (Conceptualization, Data

curation, Formal analysis, Funding acquisition, Investigation, Methodology, Project administration, Resources, Supervision, Validation, Writing—original draft, Writing—review & editing)

Supplementary material

Supplementary material is available at *Cerebral Cortex* online.

Funding

This work was supported by the PA Department of Health grant SAP# 4100083102, the National Institute on Aging grants U19 AG074866 and R24 AG073190, Foundation of the State of Rio de Janeiro (FAPERJ), National Council for Scientific and Technological Development (CNPq), as well as by intramural grants from D'Or Institute for Research and Education (IDOR); this research was supported by the Intramural Research Program of the National Institutes of Health (NIH), National Institute of Neurological Disorders and Stroke (NINDS).

Conflict of interest statement: None declared.

Data availability

The raw data supporting the conclusions of this article are available from the corresponding author on request.

References

Aja-Fernández S, Vegas-Sánchez-Ferrero G. *Statistical analysis of noise in MRI*. Cham: Springer International Publishing; 2016.

Andersson JLR, Sotiropoulos SN. An integrated approach to correction for off-resonance effects and subject movement in diffusion MR imaging. *NeuroImage*. 2016:125:1063–1078.

Bahia CP, Vianna-Barbosa RJ, Tovar-Moll F, Lent R. Terminal arbors of callosal axons undergo plastic changes in early-amputated rats. *Cereb Cortex*. 2018:29(4):1460–1472.

Edwards TJ, Fenlon LR, Dean RJ, Bunt J, Sherr EH, Richards LJ. Altered structural connectivity networks in a mouse model of complete and partial dysgenesis of the corpus callosum. *NeuroImage*. 2020:217:116868.

Foi A. Noise estimation and removal in MR imaging: the variance-stabilization approach. In: *2011 IEEE International Symposium on Biomedical Imaging: From Nano to Macro. Presented at the 2011 IEEE International Symposium on Biomedical Imaging: From Nano to Macro*. 2011. p. 1809–1814.

Gibson EM, Purger D, Mount CW, Goldstein AK, Lin GL, Wood LS, Inema I, Miller SE, Bieri G, Zuchero JB, et al. Neuronal activity promotes oligodendrogenesis and adaptive myelination in the mammalian brain. *Science*. 2014:344(6183):1252304–1252304.

Halassa MM, editors. The thalamus. In: *The thalamus*. Cambridge: Cambridge University Press; 2022. pp. i–iieditor.

Hoerder-Suabedissen A, Hayashi S, Upton L, Nolan Z, Casas-Torremocha D, Grant E, Viswanathan S, Kanold PO, Clasca F, Kim Y, et al. Subset of cortical layer 6b neurons selectively innervates higher order thalamic nuclei in mice. *Cereb Cortex*. 2018:28(5):1882–1897.

Hori Y, Schaeffer DJ, Gilbert KM, Hayrynen LK, Cléry JC, Gati JS, Menon RS, Everling S. Comparison of resting-state functional connectivity in marmosets with tracer-based cellular connectivity. *NeuroImage*. 2020:204:1–9, 116241.

Jakab A, Kasprian G, Schwartz E, Gruber GM, Mitter C, Prayer D, Schöpf V, Langs G. Disrupted developmental organization of the structural connectome in fetuses with corpus callosum agenesis. *NeuroImage*. 2015:111:277–288.

Kasprian G, Brugger PC, Schöpf V, Mitter C, Weber M, Hainfellner JA, Prayer D. Assessing prenatal white matter connectivity in commissural agenesis. *Brain*. 2013:136(1):168–179.

LaMantia AS, Rakic P. Axon overproduction and elimination in the anterior commissure of the developing rhesus monkey. *J Comp Neurol*. 1994:340(3):328–336.

Liu C, Ye FQ, Yen CC-C, Newman JD, Glen D, Leopold DA, Silva AC. A digital 3D atlas of the marmoset brain based on multi-modal MRI. *NeuroImage*. 2018:169:106–116.

Liu C, Yen CC-C, Szczupak D, Ye FQ, Leopold DA, Silva AC. Anatomical and functional investigation of the marmoset default mode network. *Nat Commun*. 2019:10(1):1975.

Liu C, Ye FQ, Newman JD, Szczupak D, Tian X, Yen CC-C, Majka P, Glen D, Rosa MGP, Leopold DA, et al. A resource for the detailed 3D mapping of white matter pathways in the marmoset brain. *Nat Neurosci*. 2020:23(2):271–280.

Liu C, Yen CC-C, Szczupak D, Tian X, Glen D, Silva AC. Marmoset brain mapping V3: population multi-modal standard volumetric and surface-based templates. *NeuroImage*. 2021:226:1–11, 117620.

Maggioni M, Katkovnik V, Egiazarian K, Foi A. Nonlocal transform-domain filter for volumetric data denoising and reconstruction. *IEEE Trans Image Process*. 2013:22(1):119–133.

Mathiasen ML, Louch RC, Nelson AD, Dillingham CM, Aggleton JP. Trajectory of hippocampal fibres to the contralateral anterior thalamus and mammillary bodies in rats, mice, and macaque monkeys. *Brain Neurosci Adv*. 2019:3:239821281987120.

Molinari M, Minciacchi D, Bentivoglio M, Macchi G. Efferent fibers from the motor cortex terminate bilaterally in the thalamus of rats and cats. *Exp Brain Res*. 1985:57(2):305–312.

Owen JP, Li Y-O, Ziv E, Strominger Z, Gold J, Bukhpun P, Wakahiro M, Friedman EJ, Sherr EH, Mukherjee P. The structural connectome of the human brain in agenesis of the corpus callosum. *NeuroImage*. 2013:70:340–355.

Parra JED, Ripoll ÁP, García JFV. Interthalamic adhesion in humans: A gray commissure? *Anat Cell Biol*. 2022:55(1):109–112.

Paul LK, Brown WS, Adolphs R, Tyszka JM, Richards LJ, Mukherjee P, Sherr EH. Agenesis of the corpus callosum: genetic, developmental and functional aspects of connectivity. *Nat Rev Neurosci*. 2007:8(4):287–299.

Pomponio R, Erus G, Habes M, Doshi J, Srinivasan D, Mamourian E, Bashyam V, Nasrallah IM, Satterthwaite TD, Fan Y, et al. Harmonization of large MRI datasets for the analysis of brain imaging patterns throughout the lifespan. *NeuroImage*. 2020:208:1–15, 116450.

Probst M. Ueber den Bau des vollständig balkenlosen Gross-hirnes sowie über Mikrogyrie und Heterotopie der grauen Substanz. *Archiv f Psychiatrie*. 1901:34(3):709–786.

Rakic P. Evolution of the neocortex: perspective from developmental biology. *Nat Rev Neurosci*. 2009:10(10):724–735.

Rayêe D, Iack PM, Christoff RR, Lourenço MR, Bonifácio C, Boltz J, Lent R, Garcez PP. The dynamics of axon bifurcation development in the cerebral cortex of typical and acallosal mice. *Neuroscience*. 2021:477:14–24.

Şahin MH, Güngör A, Demirtaş OK, Postuk Ç, Fırat Z, Ekinci G, Kadıoğlu HH, Türe U. Microsurgical and fiber tract anatomy of the interthalamic adhesion. *J Neurosurg*. 2023:1:1–10.

Santini T, Koo M, Farhat N, Campos VP, Alkhateeb S, Vieira MAC, Butters MA, Rosano C, Aizenstein HJ, Mettenburg J, et al. Analysis

of hippocampal subfields in sickle cell disease using ultrahigh field MRI. *NeuroImage*. 2021:30:1–8, 102655.

Schaeffer DJ, Hori Y, Gilbert KM, Gati JS, Menon RS, Everling S. Divergence of rodent and primate medial frontal cortex functional connectivity. *Proc Natl Acad Sci*. 2020:117(35): 21681–21689.

Schaeffer DJ, Klassen LM, Hori Y, Tian X, Szczupak D, Yen CC-C, Cléry JC, Gilbert KM, Gati JS, Menon RS, et al. An open access resource for functional brain connectivity from fully awake marmosets. *NeuroImage*. 2022:252:1–13, 119030.

Sherman SM. Thalamus plays a central role in ongoing cortical functioning. *Nat Neurosci*. 2016:19(4):533–541.

Siffredi V, Preti MG, Obertino S, Leventer RJ, Wood AG, McIlroy A, Anderson V, Spencer-Smith MM, Ville DVD. Revisiting brain rewiring and plasticity in children born without corpus callosum. *Dev Sci*. 2021;24:1–10, e13126.

Silva AC, Liu JV, Hirano Y, Leoni RF, Merkle H, Mackel JB, Zhang XF, Nascimento GC, Stefanovic B. Longitudinal functional magnetic resonance imaging in animal models. In: Modo M, Bulte JWM, editors. *Magnetic resonance neuroimaging. Methods in molecular biology*. Totowa (NJ): Humana Press; 2011. pp. 281–302.

Suárez R, Gobius I, Richards LJ. Evolution and development of interhemispheric connections in the vertebrate forebrain. *Front Hum Neurosci*. 2014:8:1–14.

Suárez R, Paolino A, Fenlon LR, Morcom LR, Kozulin P, Kurniawan ND, Richards LJ. A pan-mammalian map of interhemispheric brain connections predates the evolution of the corpus callosum. *Proc Natl Acad Sci U S A*. 2018:115(38):9622–9627.

Szczupak D, Iack PM, Liu C, IRC5 Consortium, Tovar-Moll F, Lent R, Silva AC. Direct interhemispheric cortical communication via thalamic commissures: a new white-matter pathway in the rodent brain. *Cereb Cortex*. bhab112. 2021:(10):4642–4651.

Szczupak D, Kossmann Ferraz M, Gemal L, Oliveira-Szejnfeld PS, Monteiro M, Bramati I, Vargas FR, IRC5 Consortium, Lent R, Silva AC, et al. Corpus callosum dysgenesis causes novel patterns of structural and functional brain connectivity. *Brain Commun*. 2021:3(2):1–11.

Szczupak D, Liu C, Yen CCC, Choi S-H, Meireles F, Victorino C, Richards L, Lent R, Silva AC, Tovar-Moll F. Long-distance aberrant heterotopic connectivity in a mouse strain with a high incidence of callosal anomalies. *NeuroImage*. 2020:217: 116875.

Szczupak D, Yen CC, Liu C, Tian X, Lent R, Tovar-Moll F, Silva AC. Dynamic interhemispheric desynchronization in marmosets and humans with disorders of the corpus callosum. *Front Neural Circuits*. 2020:14:1–10.

Tournier J-D, Calamante F, Connelly A. MRtrix: diffusion tractography in crossing fiber regions. *Int J Imaging Syst Technol*. 2012:22(1): 53–66.

Tournier J-D, Smith R, Raffelt D, Tabbara R, Dhollander T, Pietsch M, Christiaens D, Jeurissen B, Yeh C-H, Connelly A. MRtrix3: a fast, flexible and open software framework for medical image processing and visualisation. *NeuroImage*. 2019:202:1–17, 116137.

Tovar-Moll F, Moll J, de Oliveira-Souza R, Bramati I, Andreiuolo PA, Lent R. Neuroplasticity in human callosal dysgenesis: a diffusion tensor imaging study. *Cereb Cortex*. 2006:17(3):531–541.

Tovar-Moll F, Monteiro M, Andrade J, Bramati IE, Vianna-Barbosa R, Marins T, Rodrigues E, Dantas N, Behrens TEJ, de Oliveira-Souza R, et al. Structural and functional brain rewiring clarifies preserved interhemispheric transfer in humans born without the corpus callosum. *Proc Natl Acad Sci*. 2014:111(21):7843–7848.

Vertes RP. Analysis of projections from the medial prefrontal cortex to the thalamus in the rat, with emphasis on nucleus reuniens. *J Comp Neurol*. 2002:442(2):163–187.

Wang F, Dong Z, Tian Q, Liao C, Fan Q, Hoge WS, Keil B, Polimeni JR, Wald LL, Huang SY, et al. In vivo human whole-brain Connectom diffusion MRI dataset at 760 μm isotropic resolution. *Sci Data*. 2021:8(1):122.

Watakabe A, Skibbe H, Nakae K, Abe H, Ichinohe N, Rachmadi MF, Wang J, Takaji M, Mizukami H, Woodward A, et al. Local and long-distance organization of prefrontal cortex circuits in the marmoset brain. *Neuron*. 2023:111(14):2258–2273.e10.

Yeh F-C. Shape analysis of the human association pathways. *NeuroImage*. 2020:223:1–12, 117329.